DNA breathing dynamics under periodic forcing: Study of several distribution functions of relevant Brownian functionals

Ashutosh Dubey and Malay Bandyopadhyay
School of Basic Sciences, Indian Institute of Technology Bhubaneswar, Bhubaneswar 751007, India

(Received 25 July 2019; published 7 November 2019)

In this paper, we study DNA breathing dynamics in the presence of an external periodic force by proposing and inspecting several probability distribution functions (PDFs) of relevant Brownian functionals which specify the bubble lifetime, reactivity, and average size. We model the bubble dynamics process by an overdamped Langevin equation of broken base pairs on the Poland-Scheraga free energy landscape. Introducing an effective time-independent description for timescales larger than $\tilde{T} = \frac{2\pi}{\omega}$ (where ω is the frequency of external periodic force) and using an elegant backward Fokker-Planck method we derive closed form expressions of several PDFs associated with such stochastic processes. For instance, with an initial bubble size of x_0, we derive the following analytical expressions: (i) the PDF $P(t_f|x_0)$ of the first passage time t_f which specifies the lifetime of the DNA breathing process, (ii) the PDF $P(A|x_0)$ of the area A until the first passage time, and it provides much valuable information about the average bubble size and reactivity of the process, and (iii) the PDF $P(M)$ associated with the maximum bubble size M of the breathing process before complete denaturation. Our analysis is limited to two limits: (a) large bubble size and (b) small bubble size. We further confirm our analytical predictions by computing the same PDFs with direct numerical simulations of the corresponding Langevin equations. We obtain very good agreement of our theoretical predictions with the numerically simulated results. Finally, several nontrivial scaling behaviors in the asymptotic limits for the above-mentioned PDFs are predicted, which can be verified further from experimental observation. Our main conclusion is that the large bubble dynamics is unaffected by the rapidly oscillating force, but the small bubble dynamics is significantly affected by the same periodic force.

DOI: 10.1103/PhysRevE.100.052107

I. INTRODUCTION

Brownian motion in the presence of an external time-dependent field is ubiquitous in geophysical, environmental, and biophysical processes. One can identify numerous geophysical and environmental processes which occur under the crucial effect of external time dependence and stochastic forcing, e.g., the change between the snow-storage and snow-melt phases [1,2], outbreak of water-borne diseases [3,4], the life cycle of tidal communities [5–7], and many more. Stochastic models with time-dependent drift and constant diffusion terms are extensively used in the study of neuroscience [8–10]. Another important area where the same kind of time-dependent drift can arise is in the time evolution of stock prices in finance [11,12]. In this respect several interesting questions of wide interest can be raised, such as (i) the probability of finding the system in a certain domain at a certain instant (survival probability), (ii) the PDF of time $P(t_f|x_0)$ at which the system exits a certain domain the first time (known as first passage time t_f) starting from an initial value x_0, (iii) the PDF of area $P(A|x_0)$ before the first passage time, (iv) the PDF $P(M)$ of the maximum value of a Brownian motion (BM) process before its first passage time, and (v) the joint probability distribution $P(M;t_m)$ of the maximum value M and its occurrence time t_m before the first passage time of the BM process. The first passage time statistics for a Wiener process with an exponential time-dependent drift term are analyzed in the context of neuron dynamics in Refs. [13,14]. Also, recent studies of DNA unzipping under periodic forcing need to be mentioned [15–17]. Recently, Molini *et al.* [18] made a study on first passage statistics of BM with purely time-dependent drift and diffusion terms using a method of images.

In the present study, we investigate several PDFs relevant to different Brownian functionals associated with the DNA unzipping process in the presence of an external periodic forcing. We basically consider two different type of periodic forcing which are experimentally accessible: (a) case I: $f(x,t) = f_0\cos(\omega t)$ and (b) case II: $f(x,t) = f_0 x\cos(\omega t)$. There are several mechanisms which can lead to unzipping of the double-stranded DNA, for example, heating [19], changing the pH of the environment [20], and application of external force [21–23]. This phenomenon is usually referred to as DNA denaturation. The process starts by locally separating the double strand into single strands to form loops, or bubbles. These bubbles fluctuate in size through stepwise zipping and unzipping of the base pairs. It is very much essential to unzip a specific region of base pairs for all physiological processes involving DNA to occur, e.g., for replication, transcription, and protein binding. Recent experimental development allows us to make direct observation of the dynamics of a single DNA molecule [24,25], which ensures intense research in the field of DNA breathing dynamics under an external forcing. Also, one can investigate force-induced separation of double-stranded DNA at various temperatures using the recently developed single-molecule force spectroscopy and dynamical force

spectroscopy [24,25]. For a detail understanding of the replication and transcription processes one needs to study the force-induced separation of double-stranded DNA into single-stranded DNA. Furthermore, in living organisms, the DNA denaturation process is sometimes naturally driven by various enzymes and proteins, which can be thought of as forced unzipping of the two strands of the double helix. In this sense the artificial force-induced separation of the double-stranded DNA is a tool to mimic and understand such processes.

There are several theoretical aspects of DNA breathing dynamics, and various methods have been employed to investigate different features of the bubble dynamics. One can name several techniques: the master-equation approach [26–28], a stochastic Gillespie scheme [29], the Fokker-Planck equation approach [30,31], stochastic dynamics simulations [32,33], and the quantum-Coulomb method [34,35]. We basically consider the breathing dynamics as a random walk in the one-dimensional coordinate x, the number of broken base pairs. In our model we ignore heterogeneity in the DNA structure, and this enables us to think of the random walk as a noisy overdamped motion at a finite temperature T on the Poland-Scheraga free energy landscape, $\mathcal{F}(x) = \gamma_0 + \gamma x + ck_BT \ln x$ (all the terms are defined later). One can think of a crossover scale x_{ch} (defined later), and this implies that the random walk takes place in a potential $\sim \ln x$ for small bubbles ($x < x_{ch}$). On the other hand, the potential grows linearly with x for large bubbles ($x > x_{ch}$). Obviously, the dynamics should be different in these two regimes.

As a matter of fact, one of the objectives of this work is to advertise for the use of the well-studied backward Fokker-Planck (BFP) method [36–39] and the path decomposition (PD) method [39], which can enable us to derive all the above-mentioned quantities $P(t_f|x_0)$, $P(A|x_0)$, $P(M)$, and $P(M, t_m)$. Both the BFP and PD methods are based on the Feynman-Kac formalism [40], and both of them are used for exploring DNA breathing dynamics under time periodic forcing. Both the techniques are extensively used in studying many aspects of classical Brownian motion, as well as for exploring different problems in computer science and astronomy [36,41,42]. We extended the applications of these elegant methods to study the Brownian functionals for a BM process of DNA breathing dynamics with purely time-dependent drift and constant diffusion. Unlike the standard Fokker-Planck (FP) treatment [43–46], which yields distribution functions directly, we derive and solve differential equations for the Laplace transforms of various Brownian functionals in the BFP method. On the other hand, we can utilize the PD method to calculate the distribution functions of interest by splitting a representative path of the dynamics into parts with their appropriate weightage of each part separately. This fact is justifiable by considering the Markovian property of the dynamics.

Although we are employing an external periodic force, the problem can be reduced to an effective time-independent dynamics by following the method of Sarkar and Dattagupta [47]. The influence of a high frequency field on a classical particle was analyzed by Kapitza [48]. Then the work of Kapitza was more generalized by Landau and Lifshitz [49]. Rahav *et al.* further extended these effective dynamics for quantum systems [50,51]. As we have mentioned, our model can be described by an overdamped Langevin equation, but Jung [52] and Sarkar and Dattagupta [47] described the effective time-independent dynamics for an overdamped Brownian motion with an external rapidly oscillating periodic forcing. We follow the method introduced by Sarkar and Dattagupta [47]. Basically, the motion can be separated into a "slow part" and a "fast part" that makes a very rapid motion about the slow motion. As a result, the slow motion feels an effective time-independent potential due to the rapid motion. In our problem the DNA breathing process occurs in a microsecond [24,25], and we are applying a terahertz field. Thus, the DNA breathing process, which is occurring on a Poland-Scheraga potential, can observe an additional effective time-independent potential due to the external rapid periodic forcing.

The paper is organized as follows. In Sec. II, we discuss our model of the DNA breathing process with an external terahertz periodic field. Then we discuss several distribution functions of interest and their relevances. The BFP and PD methods are explained in short. Our discussions are limited to two regimes: (i) large bubble and (ii) small bubble. Furthermore, we investigate the DNA breathing dynamics under the influence of two types of rapidly oscillating periodic force—(a) case I: $f(x,t) = f_0 \cos(\omega t)$ and (b) case II: $f(x,t) = f_0 x \cos(\omega t)$. In Sec. III, we discuss several PDFs for our stochastic model of DNA breathing dynamics under a rapidly oscillating periodic forcing in the large bubble limit. The small bubble dynamics is illustrated in Sec. IV. We conclude our paper in Sec. V.

II. MODEL, METHODS, AND MEASURES

A. Model

At finite temperature, the overdamped Langevin equation which governs the stochastic dynamics of the DNA breathing process under a rapidly oscillating periodic forcing is given by

$$\frac{dx}{d\tau} = -D\frac{d\mathcal{F}(x)}{dx} + f(x)\cos(\omega\tau) + \tilde{\xi}(\tau), \tag{1}$$

where $f(x)$ is either a constant f_0 or a linear function of x, i.e., $f_0 x$, $\mathcal{F}(x) = \gamma_0 + \gamma x + ck_BT \ln x$ is the Poland-Scheraga free energy. Here, γ_0 is the free energy barrier to form the initial bubble, while the term γx stands for the free energy required in breaking x base pairs. The entropy loss in forming a closed polymer loop is taken into account by the term $ck_BT \ln x$, where k_B is the Boltzmann constant, T is the temperature, while c is a constant determined by the model of the interaction between loops [53]. The parameter $\gamma = \gamma_1(T_m - T)/T_m$, with $\gamma_1 = 4k_BT_r$, T_r being the reference temperature and T_m the melting temperature, is defined as that temperature at which half of the DNA molecules denatured. Further, $\tilde{\xi}(\tau)$ is a Gaussian white noise with $\langle\tilde{\xi}(\tau)\rangle$=0 and $\langle\tilde{\xi}(\tau)\tilde{\xi}(\tau')\rangle$= $2Dk_BT\delta(\tau - \tau')$, where D is a kinetic coefficient which has dimension $(k_BT)^{-1}$ s^{-1}. Using the Poland-Scheraga free energy $\mathcal{F}(x) = \gamma_0 + \gamma x + ck_BT \ln x$ in the Langevin equation (1) and redefining the time variable $t = 2Dk_BT\tau$, we get the following equation:

$$\frac{dx}{dt} = C_2 - \frac{C_1}{x} + \frac{f(x)}{2Dk_BT}\cos\left(\frac{\omega t}{2Dk_BT}\right) + \xi(t), \tag{2}$$

where $C_1 = c/2$, $C_2 = \gamma(T - T_m)/(2k_BTT_m)$, $\langle\xi(t)\rangle$=0, $\langle\xi(t)\xi(t')\rangle = \delta(t - t')$. For simplicity we assume that

$D = 1/2$ and $k_BT = 1$. This results in

$$\frac{dx}{dt} = C_2 - \frac{C_1}{x} + f(x)\cos(\omega t) + \xi(t). \tag{3}$$

B. Effective Langevin dynamics

In this section our main goal is to derive an effective time-independent Langevin equation for timescales larger than $\tilde{T} = \frac{2\pi}{\omega}$ of the real dynamics as described by Eq. (3). One can actually map the real overdamped Langevin Eq. (3) by a modified Langevin equation where the external periodic forcing is absorbed by a modified effective potential term $U_{\rm eff}(x)$. Sarkar *et al.* [47] and Jung [52] already proved that the noise term is not affected by the external periodic forcing. Hence, we can omit the noise term for the time being. Now, we decompose $x(t)$ into a fast variable $\eta(t)$ and a slow variable $X(t)$. Thus, Eq. (3) becomes

$$\dot{X}(t) + \dot{\eta}(t) = -\mathcal{F}'[X(t) + \eta(t)] + f[X(t) + \eta(t)]\cos(\omega t). \tag{4}$$

By Taylor expanding the right-hand side of the above equation, we obtain

$$\begin{aligned}\dot{X}(t) + \dot{\eta}(t) = &-\left[\mathcal{F}'(X) + \mathcal{F}''(X)\eta + \tfrac{1}{2}\mathcal{F}'''(X)\eta^2 + \cdots\right] \\ &+ f(X)\cos(\omega t) + \eta f'(X)\cos(\omega t).\end{aligned} \tag{5}$$

Since $\eta(t)$ is considered as a fast variable and $f(X) \geqslant 1$, we can demand from Eq. (5), with a very good approximation, that

$$\dot{\eta}(t) = f(X)\cos(\omega t), \tag{6}$$

which implies that $\eta(t) = \frac{f(X)}{\omega}\sin(\omega t)$. Next, we take the average over time $\tilde{T} = \frac{2\pi}{\omega}$. Over this timescale one may consider $X(t)$ and $\dot{X}(t)$ to be constant. Thus, we obtain

$$\begin{aligned}\dot{X}(t) = &-\left[\mathcal{F}'(X) + \tfrac{1}{2}\mathcal{F}'''(X)\langle\eta^2\rangle + \cdots\right] \\ &+ f'(X)\langle\eta\cos(\omega t)\rangle.\end{aligned} \tag{7}$$

(i) Case I: If we consider $f(X) = f_0$, one can show that $-\frac{1}{2}\mathcal{F}'''(X)\langle\eta^2\rangle = \frac{f_0^2}{2\omega^2}\frac{C_1}{X^3}$ and $f'(X)\langle\eta\cos(\omega t)\rangle = 0$. Thus, the effective dynamics becomes

$$\dot{X}(t) = C_2 - \frac{C_1}{X}\left(1 + \frac{f_0^2}{2\omega^2 X^2}\right). \tag{8}$$

(ii) Case II: $f(X) = f_0X$, $-\frac{1}{2}\mathcal{F}'''(X)\langle\eta^2\rangle = \frac{f_0^2}{2\omega^2}\frac{C_1}{X}$, and $f'(X)\langle\eta\cos(\omega t)\rangle = 0$. Hence, the effective dynamics becomes

$$\dot{X}(t) = C_2 - \frac{C_1}{X}\left(1 + \frac{f_0^2}{2\omega^2}\right). \tag{9}$$

For timescales larger than T and using the effective Hamiltonian method of rapidly oscillating force [47,52] one can obtain effective time-independent overdamped Langevin equations:

(i) Case I: $f(X,t) = f_0\cos(\omega t)$ where one obtains

$$\frac{dX}{dt} = C_2 - \frac{C_1}{X}\left(1 + \frac{f_0^2}{2\omega^2 X^2}\right) + \xi(t). \tag{10}$$

(ii) Case II: $f(X,t) = f_0X\cos(\omega t)$ where one obtains

$$\frac{dX}{dt} = C_2 - \frac{C_1}{X}\left(1 + \frac{f_0^2}{2\omega^2}\right) + \xi(t). \tag{11}$$

We have chosen two particular forms of external periodic forces $f_0\cos(\omega t)$ [case I] and $f_0x\cos(\omega t)$ [case II]. These are the model potential for the Paul trap and for rapidly scanning optical tweezers [54] and are very much experimentally realizable [55,56]. Thus, Eqs. (10) and (11) introduce a characteristic scale $x_{ch} = \frac{C_1}{C_2}$ such that for small bubbles, $x\langle x_{ch}$, the free energy is governed by the loop-forming term $\ln x$, and the effective Langevin dynamics of (10) and (11) is essentially governed by the term C_1. For large bubbles with $x\rangle x_{ch}$, the linear base-pair dissociation term γx dictates the dynamics, which results in the term C_2 dominating the Langevin dynamics. For $T\langle T_m$, the Langevin dynamics occurs in an attractive potential for all bubble sizes, thereby ensuring eventual bubble closure. Above T_m, large bubbles with $x\rangle x_{ch}$ grow in size under a repulsive linear potential to ultimately yield full denaturation, while a small bubble with $x\langle x_{ch}$ may evolve towards closure under the influence of the attractive $\ln x$ potential. We will utilize below the length scale x_{ch} to distinguishing between small and large bubbles.

C. Methods

In one dimension, the first passage statistics-related problem is basically formulated by considering a state variable which evolves stochastically according to a given law in its phase space. We are mainly concerned about the instant when the variable leaves a certain domain for the first time. To deal with such a problem a number of methods or approaches are described in Refs. [36,44,45,57]. Here, we describe two elegant methods: (i) the backward Fokker-Planck method and (ii) the path decomposition (PD) method.

1. Backward Fokker-Planck method

Following Ref. [36], we can introduce a general description to compute the PDF of a Brownian functional in a time interval $[0, t_f]$, where t_f is the first passage time of the process. Thus, one can introduce a functional to calculate different statistical properties of a Brownian functional:

$$B = \int_0^{t_f} U(x(\tau))d\tau, \tag{12}$$

where $x(\tau)$ is a Brownian path which follows differential equations (10) and (11) and it starts at x_0 at time $\tau = 0$ and continues up to $\tau = t_f$. Here, $U(x(\tau))$ is a specified function of the path and its form depends on the quantity we are interested in calculating. For example, if we are interested in calculating the first passage time one should choose $U(x(\tau)) = 1$. On the other hand, for the area distribution one should consider $U(x(\tau)) = x(\tau)$. One can easily understand that B is a random variable which can take different values for different Brownian paths. The main goal is to calculate the probability distribution $P(B|x_0)$. Now, one may note that the random variable B can only be positive for our choice of $U(x(\tau))$. Thus, one may consider the Laplace transform of the

distribution $P(B|x_0)$:

$$Q(x_0, p) = \int_0^\infty dT\, P(B|x_0) \exp(-pB) = \left\langle \exp\left[-p \int_0^{t_f} U(x(\tau))d\tau\right]\right\rangle. \quad (13)$$

Here, the angular bracket denote the average over all possible paths starting at $x_0 = 0$ at $\tau = 0$ and ending at the first time they cross the origin. For simplicity, we will drop the variable p in the function $Q(x_0, p)$ in the rest of our discussion. Now, to derive a differential equation for $Q(x_0)$, we follow the method described in Ref. [36]. Finally, taking the averages over the noise by using the facts $\langle \xi(0)\rangle = 0$ and $\langle \xi^2(0)\rangle = 1/\Delta\tau$ as $\Delta\tau \to 0$, one obtains, to lowest order in $\Delta\tau$, the backward Fokker-Planck differential equation of $Q(x_0)$ in the Laplace transformed space corresponding to Eqs. (10) and (11) as

$$\frac{1}{2}\frac{d^2Q(x_0)}{dx_0^2} + \left[C_2 - \frac{C_1}{x_0}\left(1 + \frac{f_0^2}{2\omega^2 x_0^2}\right)\right]\frac{dQ(x_0)}{dx_0} - pU(x_0)Q(x_0) = 0 \quad (14)$$

and

$$\frac{1}{2}\frac{d^2Q(x_0)}{dx_0^2} + \left[C_2 - \frac{C_1}{x_0}\left(1 + \frac{f_0^2}{2\omega^2}\right)\right]\frac{dQ(x_0)}{dx_0} - pU(x_0)Q(x_0) = 0, \quad (15)$$

respectively.

Boundary conditions. Equations (14) and (15) are valid in the regime $x_0 \in [0, \infty]$ with the following boundary conditions: (i) As the initial position $x_0 \to 0$, the first passage time vanishes which gives us $Q(x_0 = 0) = 1$; (ii) on the other hand, as $x_0 \to \infty$, the first passage time diverges, which results in $Q(x_0 \to \infty) = 0$.

Thus, our scheme will be as follows. We can solve the differential equations (14) and (15) with appropriate boundary conditions as mentioned above, providing us the Laplace transformed PDFs of various quantities which are determined by the choice of $U(x_0)$. Now, inverting the Laplace transform with respect to p, one can obtain the desired PDF $P(B|x_0)$. On the other hand, the standard Fokker-Planck method adopted in Refs. [44,45] yields the distribution function $P(x, t)$ directly. Thus, these two approaches are distinct, providing complementary information.

2. The path decomposition method

The basic principle of this PD method is very simple. Let us consider a simple continuous time Brownian motion evolving via $dz/d\tau = \xi(\tau)$, where $\xi(\tau)$ is a white noise with $\langle \xi(\tau)\rangle = 0$ and $\langle \xi(\tau)\xi(\tau_0)\rangle = \delta(\tau - \tau_0)$. Our motion is Markovian and one can assume that the maximum can occur at t_m, where t_m is the time at which the maximum size of the bubble is reached. One can break a typical path into two parts before (left/L) and after (right/R) t_m. Since the weights of the left and right parts of t_m are completely independent of each other, the total weight of the whole path is the product of the weights of the two split parts [36]. Here, weights W_L and W_R are the weightage of the path before and after t_m. As a matter of fact, the total weight W of the whole path is

$$W = W_L \times W_R. \quad (16)$$

Let us denote $q(z)$ the probability that the motion described by $dz/d\tau = \xi(\tau)$ exits the interval $[0, M]$ for the first time through the origin. Now, following Ref. [39] one can obtain

$$q(z) = 1 - \frac{z}{M}. \quad (17)$$

As $q(z)$ is giving us the probability that the maximum before first passage time is less than or equal to M, one can obtain the probability $P(M)$ by differentiating $q(z)$ with respect to M:

$$P(M) = \frac{z}{M^2}. \quad (18)$$

Following Ref. [39], we enforce a cutoff ϵ by considering $z(t_m) = M - \epsilon$ to avoid an infinite time crossing immediately after the first crossing and finally we take the limit $\epsilon \to 0$. As, W_R is the weight of a path that starts at $M - \epsilon$ at time t_m and exits the interval $[0, M]$ for the first time through the origin, one can say that $W_R = q(M - \epsilon)$. On the left-hand side of t_m, one needs to consider the path-integral treatment with the Feynman-Kac formula [40] which gives the weight of a path in terms of the propagator $\langle z_0|e^{-\hat{H}t_m}|M - \epsilon\rangle$, since the process propagates from z_0 at $\tau = 0$ to M at $\tau = t_m$ without crossing the level M (since M is maximum) and the level 0 (the origin) in the interval $[0, t_m]$. Finally,

$$W_L = \left(\frac{z_0}{M - \epsilon}\right)\sum_{n=1}^{\infty} e^{-E_n t_m}\psi_n(M - \epsilon)\psi_n(z_0), \quad (19)$$

where $\psi_n(z)$ and E_n are the eigenfunctions and eigenenergies, respectively, for the Hamiltonian $\hat{H} = -\frac{1}{2m}\frac{d^2}{dz^2} + V(z)$ with $V(z) = 0$ if $0 < z < M$ and $V(z) = \infty$ if $z = 0$ or $z = M$.

D. Measures

Our primary focus is on several first-passage Brownian functionals of physical relevance. In the context of DNA bubble dynamics under rapid forcing, we explore the following PDFs:

(i) First passage time or lifetime of the stochastic process. The first passage time PDF $P(t_f|x_0)$, i.e., the PDF of the time of touching the origin the first time with initial starting point x_0, provides information about the lifetime of the bubble. A related quantity is the survival probability $C(x_0, t) = 1 - \int_0^{t_f} P(t_f|x_0)dt_f$ of the process. This survival probability is an experimentally measurable quantity. For example, in the context of DNA breathing dynamics $C(x_0, t)$ can be inferred from experiments by measuring fluorescence correlations of a tagged DNA [24,25]. For the DNA breathing dynamics, our key stochastic variable is the number of broken base pairs, $x(t)$.

(ii) Area under a path. If we consider a typical path which is described by Eqs. (10) and (11), one can define the area under such a path before the first passage time as $A = \int_0^{t_f} x(t)dt$. The interesting quantity is its PDF $P(A|x_0)$ with an initial value x_0. This quantity is of interest because it provides a measure for the effectiveness of the corresponding stochastic processes. Let us consider that a binding process of protein can occur only inside the double helix, on the single-stranded

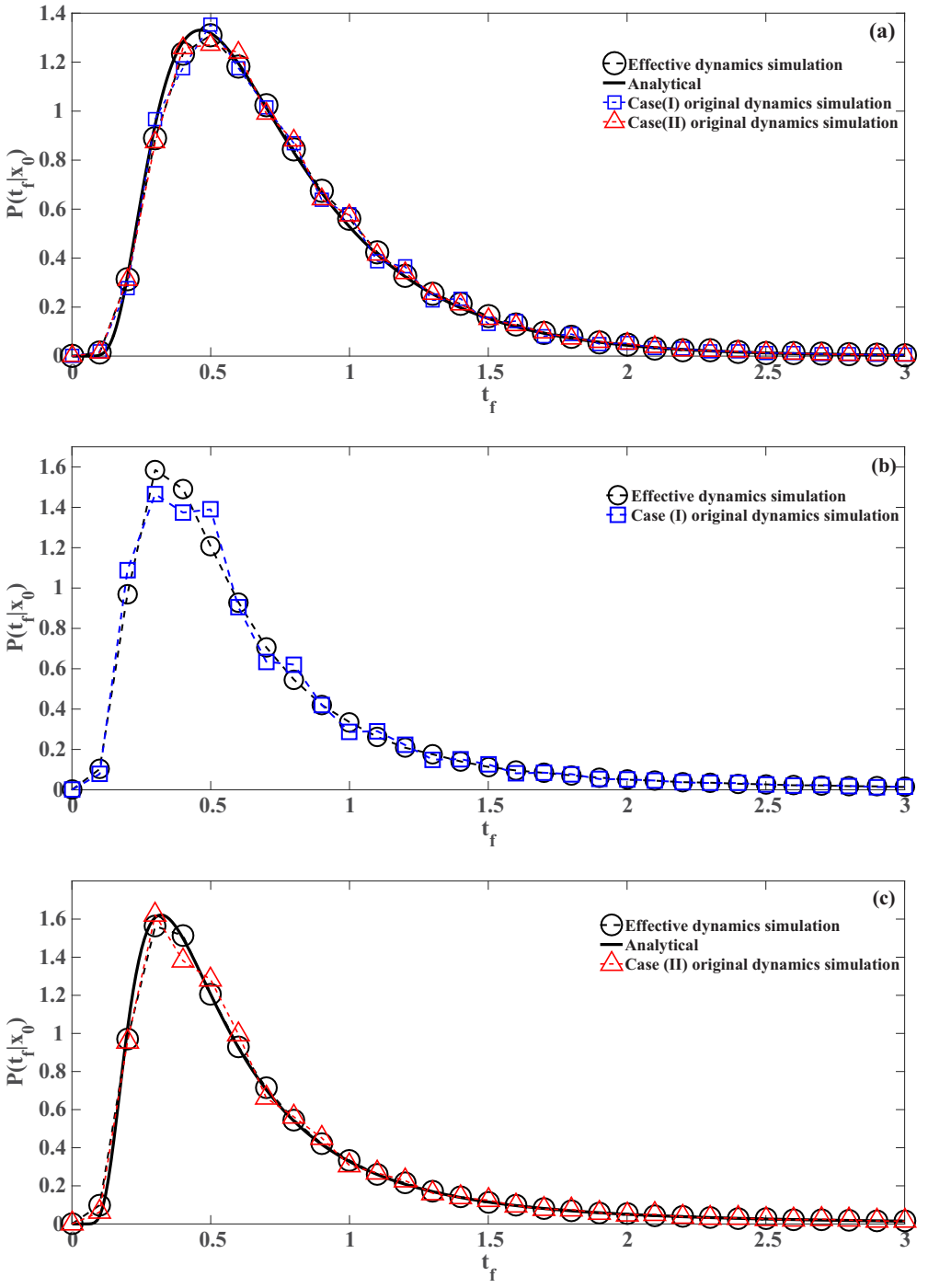

FIG. 1. Plot of PDF of first passage time $P(t_f|x_0)$ (a) for the case of large bubble dynamics with $C_2 = -2$, $x_0 = 1.5$, $f_0 = 1$, $\omega = 30$. (b, c) The case of small bubble dynamics for case I and case II, respectively, with $C_1 = 2$, $x_0 = 1.5$, $f_0 = 1$, $\omega = 20$. In all figures, the black circle denotes numerically simulated result of effective dynamics, and the black solid line is used to indicate analytical results. The blue square with dashed line and red triangle with dashed line are used to mark the numerical results of original dynamics for the periodic force $F(x,t) = f_0 \cos(\omega t)$ and $F(x,t) = f_0 x \cos(\omega t)$, respectively.

DNA. One can think of this process as facilitated with increasing bubble size as well as a sufficiently long bubble lifetime. While the first-passage time distribution provides information about the average bubble lifetime, it does not contain any hint of the average bubble size before closure. Thus, it is very much useful to propose the PDF $P(A|x_0)$ of the area A covered till the first passage time, which provides a measure of bubble reactivity by containing information about both size of the bubble and its characteristic lifetime.

(iii) Maximum size M. The other useful measure for quantifying reactivity of the process is the PDF of the maximum bubble size before the closure of the bubble, $P(M)$. Again, if we assume that a protein binding process can only take place inside the double helix and due to some geometrical

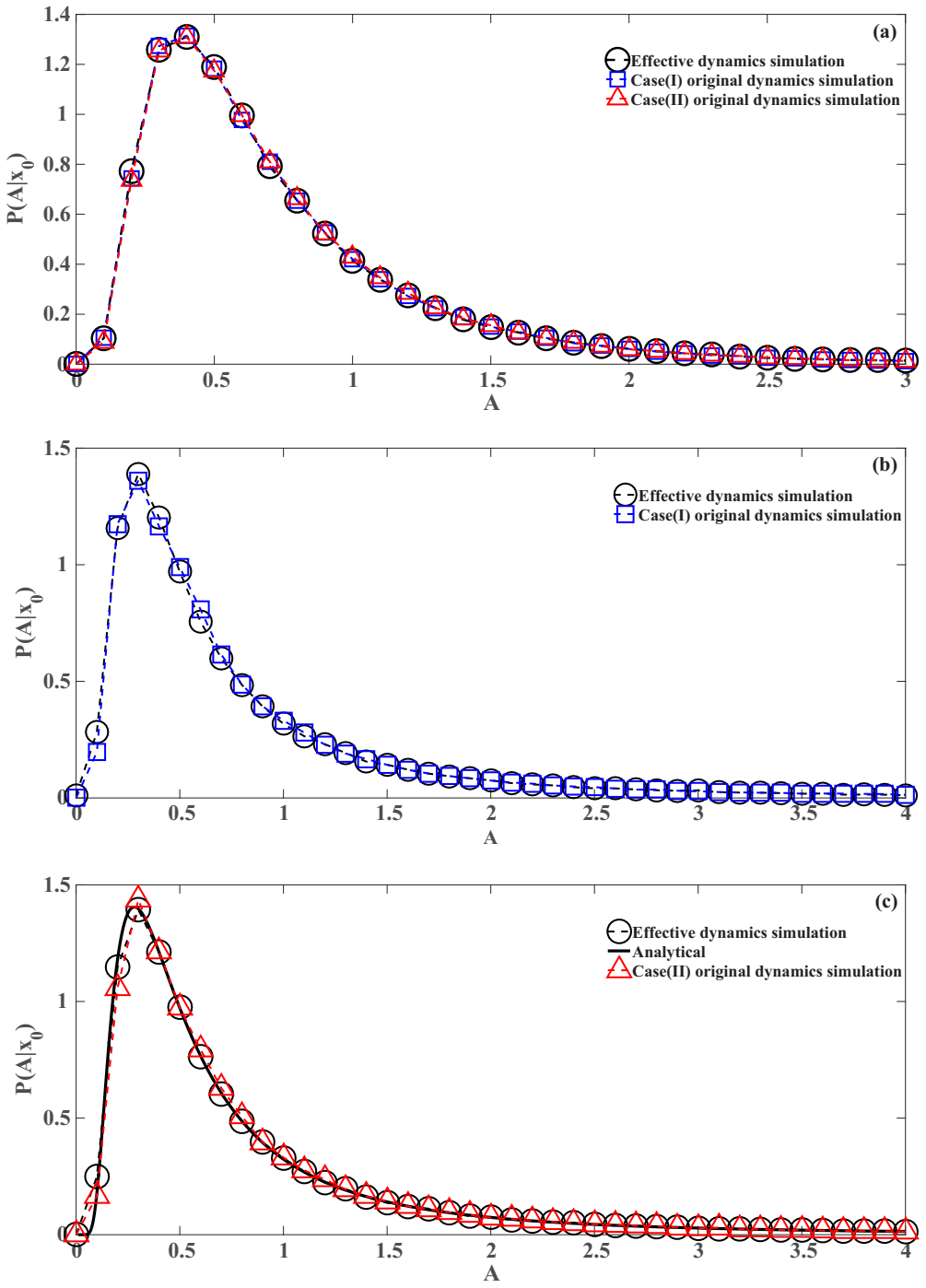

FIG. 2. Plot of PDF of area $P(A|x_0)$ until the first passage time (a) for the case of large bubble dynamics with $C_2 = -2$, $x_0 = 1.5$, $f_0 = 1$, $\omega = 30$. (b, c) The case of small bubble dynamics for case I and case II, respectively, with $C_1 = 2$, $x_0 = 1.5$, $f_0 = 1$, $\omega = 20$. Here, we use the black circle to denote numerically simulated results of effective dynamics, and the black solid line is used to indicate analytical results. Furthermore, the original dynamics for cases I and II are indicated by the blue square with dashed line and red triangle with dashed line, respectively.

constraints, the process can happen only when the bubble is large enough. If the timescale of this process is very short, shorter than the average bubble lifetime, a relevant measure for the bubble reactivity is its maximum opening before closure.

All the above-mentioned three measures, (i), (ii), and (iii), are derived below by following the backward Fokker-Planck method discussed in Sec. II B.

Maximum size M and the corresponding time t_m. The joint probability distribution function $P(M, t_m)$ can be investigated here by following the PD method, which is based on the Feynman-Kac formalism [40] (see Sec. II C). Using this PDF, one can further calculate the distribution function $P(t_m)$ of the time at which the process attains its maximum size before hitting the origin. This latter PDF is of interest because it

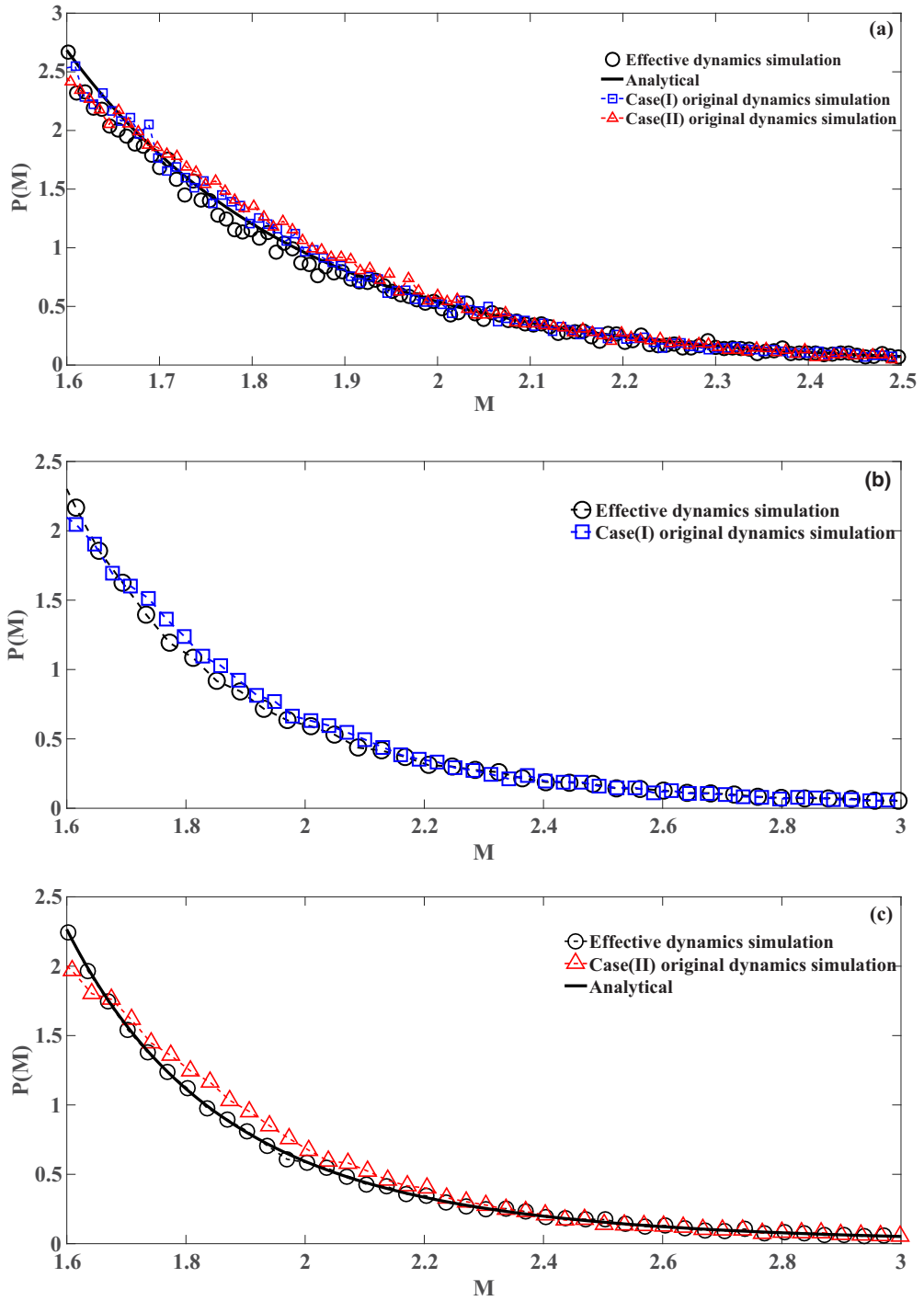

FIG. 3. Plot of PDF of maximum $P(M)$ before first passage time (a) for the case of large bubble dynamics with $C_2 = -2, x_0 = 1.5, f_0 = 1, \omega = 30$. (b, c) The case of small bubble dynamics for case I and case II, respectively, with $C_1 = 2, x_0 = 1.5, f_0 = 1, \omega = 20$. We consider the black circle to denote numerically simulated results of effective dynamics, and black solid line is used to indicate the analytical results. The blue square with dashed line indicates numerical result of original dynamics for the periodic force $F(x,t) = f_0 \cos(\omega t)$, and red triangle with dashed line is considered to signify numerical results of original dynamics for the case $F(x,t) = f_0 x \cos(\omega t)$.

provides information about the (average) time of occurrence of the largest bubble size before closure.

E. Numerical simulation

In the present work, we study different statistical properties of Brownian functionals related with the DNA breathing dynamics modeled by the following overdamped Langevin equation:

$$\frac{dx(t)}{dt} = C_2 - \frac{C_1}{x} + f(x)\cos(\omega t) + \xi(t), \tag{20}$$

where $x(t)$ is the stochastic variable of broken base pairs, the drift term $\mu(x,t) = C_2 - \frac{C_1}{x} + f(x)\cos(\omega t)$, external

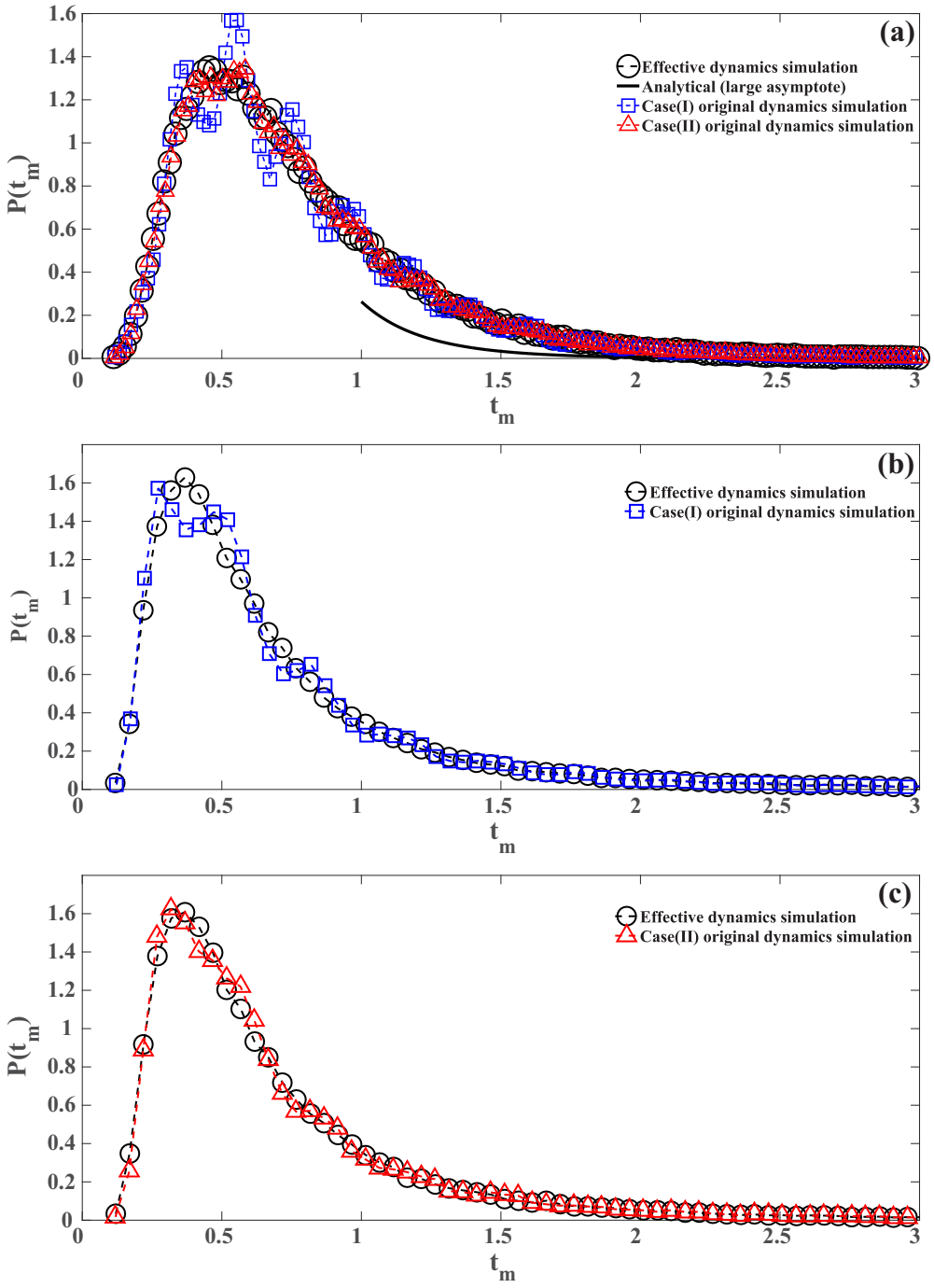

FIG. 4. Plot of PDF of time at which maximum occurs $P(t_m)$ before first passage time (a) for the case of large bubble dynamics with $C_2 = -2, x_0 = 1.5, f_0 = 1, \omega = 30$. We also plot the PDF $P(t_m)$ for small bubble dynamics in (b) and (c) for cases I and II, respectively, with $C_1 = 2, x_0 = 1.5, f_0 = 1, \omega = 20$. In all figures, the black circle denotes numerically simulated results of effective dynamics, and we consider black solid line to indicate analytical result at large asymptote. The blue square with dashed line and red triangle with dashed line are considered to signify numerical results of original dynamics for the periodic force $F(x,t) = f_0 \cos(\omega t)$ and $F(x,t) = f_0 x \cos(\omega t)$, respectively.

oscillating periodic force $f(x)\cos(\omega t)$, and $\xi(t)$ is the noise term. We consider two different experimentally realizable and interesting forms of $f(x)$—(i) case I: $f(x,t) = f_0 \cos(\omega t)$ and (ii) case II: $f(x,t) = f_0 x \cos(\omega t)$. When we are solving the exact Eq. (20) with the help of stochastic Runge-Kutta method, we label it as real dynamics. Using the Sarkar *et al.* method, one can find effective time-independent overdamped Langevin equations [for both case I Eq. (10) and case II Eq. (11)] as described previously. We call these effective dynamics. We numerically solved the exact Langevin equations as well as the time-independent effective dynamics also. The PDFs of different Brownian functionals related with different relevant quantities to characterize the breathing dynamics can be numerically simulated by solving or integrating the above-mentioned Langevin equations. We basically follow the second-order stochastic Runge-Kutta (SRK) algorithm

discussed in Ref. [58] to update the Brownian trajectory for the real dynamics. The update follows the following rule:

$$x(\Delta t) = x_0 + \frac{D(\Delta t)}{2T}\Bigg[F(x_0) + F\left(x_0 + \frac{D(\Delta t)}{T}F(x_0)\right) \times \Delta t + \Gamma_0\Bigg]\Delta t + \Gamma_0, \tag{21}$$

where $F(x_0) = C_2 - \frac{C_1}{x_0} + f(x_0)\cos(\omega \Delta t)$ with $f(x_0) = f_0$ for case I and $f(x_0) = f_0 x_0$ for case II. One can notice that Γ_0 is a random number typically sampled from a Gaussian distribution with zero mean and a width given by $\langle \Gamma_0^2 \rangle = 2D\Delta t$. For our purpose to simulate different PDFs of Brownian functionals we consider $\Delta t = 10^{-3}$. Usually we consider 2×10^5 number of paths which starts from a particular point x_0 and ends close to the origin within a preassigned tolerance level and taking averages over all the 2×10^5 number of realizations. Then, we calculate the required PDFs for different Brownian functionals to compare with our analytical predictions. The update of the Brownian trajectory for the effective dynamics also follows the above Eq. (21), but $F(x_0)$ will be different compared to real dynamics. For the effective dynamics, $F(x_0) = C_2 - \frac{C_1}{x_0}(1 + \frac{f_0^2}{2\omega^2 x_0^2})$ is for case I and for case II it is $F(x_0) = C_2 - \frac{C_1}{x_0}(1 + \frac{f_0^2}{2\omega^2})$.

Now we describe how to compute the four PDFs. To compute a first-passage time distribution, we first let the system evolve according to Eq. (21), starting from some specified initial point. Due to restrictions arising from numerical computation, we consider that when the position of particles is less then 10^{-4} (tolerance level) it touches the origin and consider it to be the first passage time of the corresponding trajectory. So we note the corresponding time when the particle reaches that limit for each realization and repeat the same process for all realizations. Once we have the first-passage time data for all realizations, data binning was carried out with a bin size of 0.1 with subsequent normalization to plot the normalized probability distribution function for the first passage time. Again, starting from some specified initial point, we let the system evolve as stated in Eq. (21) and the area under the curve is computed until the first passage time for each realization and we store the corresponding value of A. This procedure is repeated for all realizations (2×10^5 nos.) and we store all the corresponding areas until the first passage time. Then, again following the data binning procedure with a bin size 0.1, we plot the PDF for area. To compute $P(M)$, we update the trajectory according to Eq. (21) and find the maximum value of $x(t)$ between the starting point and the first passage time. This procedure is repeated for all the realizations, and we store the maximum value (M) and the corresponding time (t_m) for each realization. Again following the binning procedure we can plot the PDF for maximum $P(M)$ and the PDF of the corresponding time $P(t_m)$.

III. LARGE BUBBLE DYNAMICS

In this section we analytically derive the closed form expressions of four PDFs mentioned in Sec. II C. Our analytical results are obtained based on the effective time-independent Langevin equations (10) and (11) for the two cases. Since the theoretical calculations are not exact for model (3), it is important to test its accuracy against the true PDFs obtained by numerically solving original dynamics Eq. (10) and (11). First, we investigate the dynamics of large bubbles of size $x > x_{ch}$. In this limit, one can neglect the term $-\frac{C_1}{x}$ in the Langevin equation (3) and study the dynamics dictated by the effective Langevin equation:

$$\frac{dx}{dt} = C_2 + \xi(t). \tag{22}$$

Thus, the corresponding backward Fokker-Planck equation becomes

$$\frac{1}{2}\frac{d^2Q}{dx_0^2} + C_2\frac{dQ(x_0)}{dx_0} - pU(x_0)Q(x_0) = 0. \tag{23}$$

A. First passage time PDF: $P(t_f|x_0)$

Let us first calculate the PDF of first passage time $P(t_f|x_0)$ by substituting $U(x_0) = 1$ in Eq. (23) and using proper boundary conditions $Q(x_0 = 0) = 1$ and $Q(x_0 \to \infty) = 0$, where we obtain

$$Q(x_0, p) = \exp\big[-x_0\big(C_2 + \sqrt{2p + {C_2}^2}\big)\big]. \tag{24}$$

By taking the inverse Laplace transform of the above equation (24) [59], we get the PDF of the first passage time (see Fig. 1(a) where we found a very good agreement between theoretical result [Eq. (25)] and numerical result)

$$P(t_f|x_0) = \frac{x_0}{\sqrt{2\pi}t_f^{3/2}}\exp\left(-\frac{(x_0 + C_2 t_f)^2}{2t_f}\right). \tag{25}$$

The moments $\langle t_f^k \rangle >$ are given by

$$\langle t_f^k \rangle = \sqrt{\frac{2}{\pi}}\left(\frac{x_0}{|C_2|}\right)^k (x_0|C_2|)^{\frac{1}{2}} e^{-x_0 C_2} K_{k-1/2}(x_0|C_2|). \tag{26}$$

Now, using the fact that [60] $K_{1/2}(x) = \sqrt{\frac{\pi}{2x}}e^{-x}$, the mean first passage time can be obtained as $\langle t_f \rangle = x_0\frac{e^{-2C_2x_0}}{C_2}$ for $C_2 > 0$ and $\langle t_f \rangle = \frac{x_0}{|C_2|}$ for $C_2 < 0$. Then the next step is to calculate the survival probability, which is given by

$$C(x_0, t) = 1 - \frac{x_0}{\sqrt{2\pi}}e^{-C_2x_0}\int_0^t dt_f \frac{e^{-(\frac{x_0^2}{2t_f} + C_2{}^2 t_f)}}{t_f^{\frac{3}{2}}}. \tag{27}$$

If we consider $C_2 < 0$ (with $T < T_m$), it can be shown that for large $t \to \infty$,

$$C(x_0, t) = 1 - \frac{C_2 x_0}{2\sqrt{\pi}}e^{-C_2x_0 - \frac{x_0^2}{2t}}\left[\Gamma\left(-\frac{1}{2}\right) - \Gamma\left(-\frac{1}{2}, \frac{{C_2}^2 t}{2}\right)\right]. \tag{28}$$

B. PDF of area until the first passage time: $P(A|x_0)$

One may understand that the PDF $P(t_f|x_0)$ can supply the important information about the lifetime of the bubble, but it cannot give us information about the average bubble size. The PDF $P(A|x_0)$ will supply us useful information about the readiness to react under different conditions. So we now discuss how to obtain the PDF $P(A|x_0)$.

We can compute the distribution of A, i.e., $P(A|x_0)$, by considering the following backward Fokker-Planck equation [using Eq. (23) with $U(x_0) = x_0$)] [39,41] with boundary conditions (i) $Q(x_0 \to \infty) = 0$ and (ii) $Q(x_0 = 0) = 1$:

$$\frac{1}{2}\frac{d^2Q(x_0)}{dx_0^2} + C_2\frac{dQ(x_0)}{dx_0} - px_0Q(x_0) = 0. \tag{29}$$

Now, using the transformation $Q(x_0) = e^{-C_2x_0}\hat{Q}(x_0)$, we get

$$\frac{d^2\hat{Q}}{dx_0^2} - \left(2px_0 + {C_2}^2\right)\hat{Q} = 0. \tag{30}$$

Now, applying boundary conditions (a) $Q(x_0) = 0$ when $x_0 \to \infty$ and (b) $Q(x_0) = 1$ when $x_0 \to 0$, we get the general solution of Eq. (30):

$$Q(p, x_0) = \frac{e^{-C_2x_0}Ai\left(2^{1/3}p^{1/3}x_0 + \frac{{C_2}^2}{2^{2/3}(p)^{2/3}}\right)}{Ai\left(\frac{{C_2}^2}{2^{2/3}(p)^{2/3}}\right)}, \tag{31}$$

where $Ai(x)$ is the Airy function [61]. It is impossible to make the exact inverse Laplace transform of Eq. (31). Hence, we will try to get the PDF at two asymptotes.

Case I: $P(A|x_0)$ as $A \to 0$

$$Q(p, x_0, t) = \frac{e^{-C_2x_0}Ai(2^{1/3}(p)^{1/3}x_0)}{Ai(0)} \sim K_{1/3}\left(\frac{2}{3}2^{1/2}x_0^{3/2}(p)^{1/2}\right). \tag{32}$$

Now, using the identity

$$\int_0^\infty drr^{\nu-1}e^{-\alpha r-\frac{\beta}{r}} = 2\left(\frac{\beta}{\alpha}\right)^{\nu/2}K_\nu(2\sqrt{\alpha\beta}) \tag{33}$$

we get $\nu = 1/3$, $\alpha = p$, and $\beta = \frac{2x_0^3}{9}$. Finally, we can obtain the PDF $P(A|x_0)$ for $A \to 0$:

$$P(A|x_0) \sim \frac{2^{1/3}}{3^{2/3}\Gamma(1/3)}\frac{x_0e^{-C_2x_0}}{(A)^{4/3}}e^{-2x_0^3/9A}. \tag{34}$$

Case II: Following Ref. [39], one can obtain the area distribution for $A \to \infty$:

$$P(A|x_0) \sim \left(\frac{2{C_2}^3}{3\pi^2A^3}\right)^{1/4}e^{-C_2x_0}\sinh(|C_2|x_0)e^{-(8A|C_2|^3/3)^{1/2}} \tag{35}$$

We have seen very good agreement with the numerical results with that of the theoretical prediction at asymptotic limits [see Fig. 2(a)].

C. Probability distribution of maximum $P(M)$

The probability distribution of maximum before first passage time, $P(M)$, provides important information about the maximum bubble size before complete closure. In that sense it is one of the important quantities to study. Let us consider $Q(x_0)$ as the probability that a Brownian particle starting from x_0 and described by Eq. (22) exits the interval $x \in [0, M]$ for the first time through the origin. Hence, we can say that $Q(x_0)$ is the cumulative probability that the maximum before the first passage time is $\leqslant M$. Also, this function satisfies two boundary conditions: (i) $Q(x_0 = 0) = 1$ and (ii) $Q(x_0 = M) = 0$. Now, considering $\phi_{\Delta\tau}(\Delta x)$ as the distribution function of a small displacement Δx in time, $\Delta\tau \to 0$. Using the Markovian property of the dynamics (14), one can write

$$Q(x_0) = \int d(\Delta x)Q(x_0 + \Delta x)\phi_{\Delta\tau}(\Delta x). \tag{36}$$

Now, using Taylor expansion of $Q(x_0 + \Delta x)$ and averaging over $\Delta x = 2C_2\Delta\tau + \xi(0)\Delta\tau$ with $\langle\xi(0)\rangle = 0$ and $\langle\xi^2(0)\rangle = 1/\Delta\tau$ (to leading order in $\Delta\tau$) we obtain

$$\frac{d^2Q}{dx_0^2} + 2C_2\frac{dQ}{dx_0} = 0. \tag{37}$$

One can easily observe that one can recover Eq. (37) from our central Eq. (23) by considering $U(x_0) = 0$. The solution of Eq. (37) with the help of the above-mentioned boundary conditions is given by

$$Q(x_0) = \frac{\sinh[C_2(M - x_0)]}{\sinh(C_2M)}e^{-C_2x_0}. \tag{38}$$

By differentiating $Q(x_0)$ with respect to M we obtain

$$P(M) = \frac{C_2\sinh(C_2x_0)}{\sinh^2(C_2M)}e^{-C_2x_0}. \tag{39}$$

Figure 3(a) shows an excellent agreement between analytical expression [Eq. (39)] and numerical results.

D. Joint PDF of the maximum M and corresponding time t_m: $P(M, t_m)$

The joint distribution of the maximum bubble size M and its occurrence time t_m can be computed using the path decomposition (PD) method discussed in Sec. II B. We can split a typical Brownian path evolving under Eq. (22) into two parts, before and after the time t_m, and their respective weights are W_L and W_R, respectively. The total weight of the whole path W is the product of the weights for the split parts $W = W_L \times W_R$. Therefore, on the right side of $t = t_m$ one is able to find the weight of a path W_R which starts at $M - \epsilon$ and leaves the interval $[0, M]$ first time through zero can be obtained from Eq. (38) and is given by

$$Q(M - \epsilon) = \frac{\sinh(C_2\epsilon)}{\sinh(C_2M)}e^{-C_2(M-\epsilon)}. \tag{40}$$

On the left-hand side of t_m. We use the path-integral method as discussed in Sec. II. The weight of the path can be given in terms of the propagator $\langle x_0|e^{-\hat{H}t_m}|M - \epsilon\rangle$ by following Feynman-Kac formula [36]:

$$\langle x_0|\exp(-\hat{H}t_m)|M - \epsilon\rangle = \sum_{n=1}^{\infty}\psi_n(M - \epsilon)\psi_n(x_0)e^{-E_nt_m}, \tag{41}$$

where $\psi_n(x)$ is the eigenfunction of the free particle. Finally, following [36,62,63] we obtain

$$P(M, t_m) = \frac{2C_2Me^{[-\frac{(\tilde{C}_2)^2}{2}t_m - \tilde{C}_2x_0]}}{\sinh[C_2M]}\frac{\pi}{M^3} \times \sum_{n=1}^{\infty}(-1)^{n+1}n\sin\left(\frac{n\pi x_0}{M}\right)\exp\left(-\frac{n^2\pi^2}{2M^2}t_m\right). \tag{42}$$

One will be really tempted to recover the marginal probability density of the maximum $P(M)$ by taking integration over t_m, or one can obtain marginal distribution $P(t_m)$ by integrating over M. But it is not possible to obtain closed form expressions of $P(t_m)$. But one can be able to extract the asymptotic behavior of $P(t_m)$. The marginal distribution $P(t_m)$ can be obtained by integrating $P(M, t_m)$ over M from x_0 to infinity. The large-t_m and small-t_m asymptotic behaviors of $P(t_m)$ for $C_2 < 0$ are discussed in Ref. [36].

(i) Large-t_m asymptote:

$$P(t_m) \sim \left[2\sqrt{\frac{2}{3}}\pi^{5/6}x_0(C_2)^{4/3}e^{-(C_2)x_0}\right]t_m^{-5/6} \times \exp\left(-\frac{(C_2)^2 t_m}{2} - \frac{3}{2}[(C_2)\pi]^{2/3}t_m^{1/3}\right). \quad (43)$$

(ii) Small-t_m asymptote:

$$P(t_m) \sim \frac{C_2 M e^{-C_2 x_0 - \frac{C_2^2}{2}t_m}}{\sqrt{2\pi t_m}\sinh(C_2 x_0)}. \quad (44)$$

The asymptotic behavior in large t_m matches with numerical results [see Fig. 4(a)].

IV. SMALL BUBBLE DYNAMICS

We analyze in this section the dynamics for small bubbles, with $x < x_{ch}$, at all temperatures, $T \neq T_m$. The analysis is also applicable for bubbles of all sizes at precisely the melting temperature T_m. In these cases, the logarithmic entropic term in the free energy (1) dictates the dynamics, which results in the Langevin equation.

Case I: $F(x,t) = f_0\cos(\omega t)$.

The effective time-independent Langevin equation in this case is given by

$$\frac{dx}{dt} = -\frac{C_1}{x}\left(1 + \frac{f_0^2}{2\omega^2 x^2}\right) + \xi(t). \quad (45)$$

The corresponding backward Fokker-Planck equation can be written as follows:

$$\frac{1}{2}\frac{d^2Q}{dx_0^2} - \frac{C_1}{x}\left(1 + \frac{f_0^2}{2\omega^2 x^2}\right)\frac{dQ(x_0)}{dx_0} - pU(x_0)Q(x_0) = 0. \quad (46)$$

Unfortunately, we are unable to derive the closed form expressions for different PDFs in this case I. Hence we numerically calculate the PDFs using both real dynamics as well as for the effective dynamics. Then we compare simulated results of real and effective dynamics for $P(t_f|x_0)$, $P(A|x_0)$, $P(M)$, and $P(t_m)$ in Figs. 1(b), 2(b), 3(b), and 4(b), respectively.

Case II: $F(x,t) = f_0 x\cos(\omega t)$.

In this case, our effective Langevin equation is given by

$$\frac{dx}{dt} = -\frac{C_1}{x}\left(1 + \frac{f_0^2}{2\omega^2}\right) + \xi(t). \quad (47)$$

The corresponding characteristic backward Fokker-Planck equation which we need to solve is

$$\frac{1}{2}\frac{d^2Q(x_0)}{dx_0^2} - \frac{\tilde{C}_1}{x_0}\frac{dQ(x_0)}{dx_0} - pU(x_0) = 0, \quad (48)$$

where $\tilde{C}_1 = C_1(1 + \frac{f_0^2}{2\omega^2})$, and the boundary conditions are $(i) Q(x_0 \to \infty) = 0$ and (ii) $Q(x_0 = 0) = 1$.

A. First passage time $P(t_f|x_0)$

To find the closed form expression for the PDF of first passage time we need to substitute $U(x_0) = 1$ in the backward Fokker-Planck equation (48), and the general solution of Eq. (48) with the substitution $U(x_0) = 1$ is

$$Q(x_0) = x_0^{\beta}[AI_\beta(\sqrt{2p}x_0) + BK_\beta(\sqrt{2p}x_0)], \quad (49)$$

where $I_\beta(x)$ and $K_\beta(x)$ are the modified Bessel function of the first and second kind, respectively, and $\beta = \tilde{C}_1 + 1/2$. A and B are arbitrary constants which are to be determined from boundary conditions. In order to satisfy $Q(x_0 \to \infty) = 0$, one needs $A = 0$, as we have $I_\beta(x) \sim \frac{e^x}{\sqrt{2\pi x}}$ and $K_\beta(x) \sim \sqrt{\frac{\pi}{2x}}e^{-x}$. Next, we know that $K_\beta(x) \sim \frac{2^{\beta-1}\Gamma(\beta)}{x^\beta}$ for $x \to 0$. Thus, the second boundary condition implies $B = \frac{\sqrt{2p}^{\tilde{C}_1+1/2}}{\Gamma(\tilde{C}_1+\frac{1}{2})2^{\tilde{C}_1-\frac{1}{2}}}$. Thus, we obtain

$$Q(x_0) = x_0^{\tilde{C}_1+1/2}\frac{(\sqrt{2p})^{\tilde{C}_1+1/2}}{\Gamma(\tilde{C}_1+1/2)2^{\tilde{C}_1-1/2}}K_{\tilde{C}_1+1/2}(\sqrt{2p}x_0). \quad (50)$$

In order to find the PDF $P(t_f|x_0)$ one needs to take the inverse Laplace transform of $Q(x_0)$ Eq. (50) by using the following identity of the inverse Laplace transform $\mathcal{L}^{-1}[a^{-n/2}p^{n/2}K_n(2\sqrt{ap})] = t^{-n-1}e^{-a/t}/2$ [59], where one finds

$$P(t_f|x_0) = \frac{x_0^{2\tilde{C}_1+1}}{\Gamma(\tilde{C}_1+1/2)2^{\tilde{C}_1+1/2}}t_f^{-\tilde{C}_1-3/2}e^{-x_0^2/2t_f}. \quad (51)$$

Equation (51) is compared with simulated results in Fig. 1(c). Besides the PDF $P(t_f|x_0)$, the other experimentally relevant quantities are the moments $\langle t_f^k\rangle$ and the survival probability. First we derive the closed form expression of moments. The moments can be obtained from the PDF $P(t_f|x_0)$:

$$\langle t_f^k\rangle = \int_0^\infty t_f^k P(t_f|x_0)dt_f = \frac{x_0^{2k}}{2^k}\frac{\Gamma(\tilde{C}_1 - k + 1/2)}{\Gamma(\tilde{C}_1 + 1/2)}, \quad (52)$$

which is valid for $k > \tilde{C}_1 + 1/2$. For $k < \tilde{C}_1 + 1/2$ the moment $\langle t_f^k\rangle$ diverges. To obtain $\langle t_f^k\rangle$ we use the identity $\int_0^\infty x^{\nu-1}\exp(-\mu x^p) = \frac{1}{|p|}\mu^{-\nu/p}\Gamma(\nu/p)$ for $\mathrm{Re}(\mu) > 0$ and $\mathrm{Re}(\nu) > 0$. The other quantity which is of experimental interest is the survival probability or the persistence of the bubble. The survival probability is defined as $C(x_0,t) = 1 - \int_0^\infty dt_f P(t_f|x_0)$. Thus, the survival probability is given by

$$C(x_0,t) = 1 - \int_0^t dt_f P(t_f|x_0) = 1 - \frac{\Gamma\left(\tilde{C}_1 + 1/2, x_0^2/2t\right)}{\Gamma(\tilde{C}_1 + 1/2)}, \quad (53)$$

where $\Gamma(s,x) = \int_x^\infty dt\, t^{s-1}\exp(-t)$ is the upper incomplete function. One can easily obtain the asymptotic behavior of $C(x_0,t)$. In the $t \to \infty$ limit one obtains

$$C(x_0,t) \approx \frac{\left(x_0^2\right)^{\tilde{C}_1+1/2}}{(\tilde{C}_1+1/2)\Gamma(\tilde{C}_1+1/2)}t^{-\tilde{C}_1-1/2}, \quad (54)$$

and in the limit $t \to 0$

$$C(x_0,t) \approx 1 - \frac{\left(x_0^2/2\right)^{\tilde{C}_1+1/2}}{\Gamma(\tilde{C}_1+1/2)} t^{-\tilde{C}_1-1/2} e^{-x_0^2/2t}. \quad (55)$$

B. Area until first passage time $P(A|x_0)$

In this section we calculate the area under the random Brownian motion Eq. (47) which starts at x_0 and continues till the first passage time. This quantity gives us information regarding the bubble's readiness to react. We substitute $U(x_0) = x_0$ in the backward Fokker-Planck Eq. (48) to compute the PDF of area $P(A|x_0)$ and obtain

$$\frac{1}{2}\frac{d^2Q(x_0)}{dx_0^2} + \frac{\tilde{C}_1}{x_0}\frac{dQ(x_0)}{dx_0} - px_0Q(x_0) = 0. \quad (56)$$

The general solution of the above equation is given by

$$Q(x_0) = \left(\frac{\sqrt{2p}}{3}\right)^{\nu} x_0^{3\nu/2}\left[B_1\Gamma(1-\nu)I_{-\nu}\left(\frac{2\sqrt{2p}}{3}x_0^{3/2}\right) + B_2(-1)^{\nu}\Gamma(1+\nu)I_{\nu}\left(\frac{2\sqrt{2p}}{3}x_0^{3/2}\right)\right], \quad (57)$$

where $\nu = (2\tilde{C}_1+1)/3$, $J_\nu(x)$, $I_\nu(x)$ is the modified Bessel function of the first kind, and B_1 and B_2 are arbitrary constants which need to be determined by applying boundary conditions. One can notice that for large x, the modified Bessel function of the first kind behaves like $I_\nu(x) \sim \frac{e^x}{\sqrt{2\pi x}}$. Thus, the boundary condition $Q(x_0 \to \infty) = 0$ implies $B_1\Gamma(1-\nu) = -(-1)^{\nu}B_2\Gamma(1+\nu)$. Thus, we obtain

$$Q(x_0) = \left(\frac{\sqrt{2p}}{3}\right)^{\nu} x_0^{3\nu/2}B_1\Gamma(1-\nu)\left[I_{-\nu}\left(\frac{2\sqrt{2p}}{3}x_0^{3/2}\right) - I_{\nu}\left(\frac{2\sqrt{2p}}{3}x_0^{3/2}\right)\right]. \quad (58)$$

To satisfy the boundary condition $Q(x_0 = 0) = 1$, we note that as $x_0 \to 0$, one has $I_\nu(x) \sim \frac{1}{\Gamma(1+\nu)}\left(\frac{x}{2}\right)^{\nu}$, which gives $B_1 = 1$. Thus, we finally have

$$\begin{aligned} Q(x_0) &= \left(\frac{\sqrt{2p}}{3}\right)^{\nu} x_0^{3\nu/2}\Gamma(1-\nu)\left[I_{-\nu}\left(\frac{2\sqrt{2p}}{3}x_0^{3/2}\right) - I_{\nu}\left(\frac{2\sqrt{2p}}{3}x_0^{3/2}\right)\right] \\ &= \left(\frac{\sqrt{2p}}{3}\right)^{\nu} x_0^{3\nu/2}\Gamma(1-\nu)\frac{2}{\pi}\sin(\nu\pi)K_{\nu}\left(\frac{2\sqrt{2p}}{3}x_0^{3/2}\right) \\ &= \left(\frac{\sqrt{2p}}{3}\right)^{\nu} x_0^{3\nu/2}\frac{2}{\Gamma(\nu)}K_{\nu}\left(\frac{2\sqrt{2p}}{3}x_0^{3/2}\right), \end{aligned} \quad (59)$$

where, in obtaining the second to the last line, we have used the identity $K_\alpha(x) = \frac{\pi}{2}\frac{I_{-\alpha}(x)-I_\alpha(x)}{\sin(\alpha\pi)}$. In arriving at the last line we use the identity $\Gamma(\alpha)\Gamma(1-\alpha) = \frac{\pi}{\sin(\alpha\pi)}$. Now, to derive $P(A|x_0)$, we need to take the inverse Laplace transform of Eq. (59) and using $\mathcal{L}^{-1}[a^{-n/2}p^{n/2}K_n(2\sqrt{ap})] = t^{-n-1}e^{-a/t}/2$ [59] we finally obtain the following by replacing ν in terms of $\tilde{C}_1$:

$$P(A|x_0) = \frac{2^{(2\tilde{C}_1+1)/3}x_0^{2\tilde{C}_1+1}}{3^{(4\tilde{C}_1+2)/3}\Gamma[(2\tilde{C}_1+1)/3]}\frac{\exp\left(-2x_0^3/9A\right)}{A^{(2\tilde{C}_1+4)/3}}. \quad (60)$$

This expression matches well with the numerical results obtained by directly simulating the Langevin equation (11) and effective dynamics [Eq. (47)] [see Fig. 2(c)].

C. Distribution of maximum before the first passage time: $P(M)$

The quantity we examine next is the probability density $P(M)$ for obtaining a bubble of maximal size M before its first closure, given that the initial size of the bubble is fixed at $x_0 \in [0, M]$. To do this, we closely follow the procedure in Ref. [36]. Let $q(x_0)$ be the probability that the motion described by Eq. (47), starting from $x_0 \in [0, M]$, exits this interval for the first time through the origin, i.e., $q(x_0)$ is the probability that the maximum before the first passage time is $\leqslant M$. This quantity is important in answering the question of how large the bubble can grow before it closes with an initial bubble size of x_0. This is of importance in calculating the efficiency of processes that can occur inside big loops only. It is evident from the definition of $q(x_0)$ that it satisfies the two boundary conditions: (i) $q(0) = 1$ and (ii) $q(M) = 0$. Considering $\phi_{\Delta\tau(\Delta x)}$ as the distribution function of a small displacement Δx in time $\Delta\tau \to 0$, we have

$$q(x_0) = \int q(x_0+\Delta x)\phi_{\Delta\tau(\Delta x)d(\Delta x)}. \quad (61)$$

On Taylor expanding $q(x_0+\Delta x)$ and then averaging over $\Delta x = -\frac{\tilde{C}_1}{x_0}\Delta\tau + \xi(0)\Delta\tau$, using $\langle\xi(0)\rangle = 0$, $\langle\xi^2(0)\rangle = \frac{1}{\Delta\tau}$, we finally get, to leading order in $\Delta\tau$,

$$\left[\frac{1}{2}\frac{d^2q(x_0)}{dx_0^2} - \frac{\tilde{C}_1}{x_0}\frac{dq(x_0)}{dx_0}\right]\Delta\tau = 0. \quad (62)$$

Since $\Delta\tau$ is arbitrary we have

$$\left[\frac{1}{2}\frac{d^2q(x_0)}{dx_0^2} - \frac{\tilde{C}_1}{x_0}\frac{dq(x_0)}{dx_0}\right] = 0, \quad (63)$$

and with the boundary conditions, the general solution is given by

$$q(x_0) = 1 - \left(\frac{x_0}{M}\right)^{(2\tilde{C}_1+1)}. \quad (64)$$

The PDF of interest is obtained by differentiating $q(x_0)$ with respect to M,

$$P(M) = \frac{(2\tilde{C}_1+1)x_0^{2\tilde{C}_1+1}}{M^{2\tilde{C}_1+2}}. \quad (65)$$

In Fig. 3(c), we compare this analytic result with numerical simulations using the real dynamics as well as the effective dynamics and observe a very good agreement for $\frac{\tilde{C}_1}{|C_2|} > x_0$ and $C_2 < 0$, as expected.

D. Joint PDF of maximum M and the corresponding time t_m: $P(M, t_m)$

In this section, we compute the joint probability distribution $P(M, t_m)$ for the motion represented by Eq. (47) with the motion starting at x_0 at time $t = 0$. Here M, denoting the maximum before the first passage time t_f, occurs at the time instant $t_m < t_f$. Note that M, t_m, and t_f are all random variables. To proceed further, we closely follow [39]. We have

to find the weight of paths that start at x_0, reach the level $M-\epsilon$ at time t_m, reach the level 0 for the first time at time $t_f > t_m$, and have a maximum less than or equal to M for all times intermediate between 0 and t_f. Here, ϵ is a small cutoff that we will eventually let go to zero. Because the motion in Eq. (47) is Markovian, the desired weight is given by the product of two factors: (1) W_L, the weight of paths that start at x_0, reaching level $M-\epsilon$ at $t=t_m$ without crossing the level M and the level 0 for intermediate times, and (2) W_R, the weight of paths that start at $M-\epsilon$ at $t=t_m$ and reach 0 at $t=t_f$ (where $t_f > t_m$), without crossing the level M and the level 0 in between. On the other hand, $q(x_0)$ in Eq. (64) is the probability for a path starting at $x_0 \in [0, M]$ to exit the interval for the first time through the origin. We can then demand that $W_R = q(M-\epsilon)$. Thus, the weight of the right path is

$$W_R = 1 - \frac{(M-\epsilon)^{(2\tilde{C}_1+1)}}{M^{2\tilde{C}_1+2}} = \frac{(2\tilde{C}_1+1)\epsilon}{M} + O(\epsilon^2), \quad (66)$$

where the last relation has been obtained assuming ϵ is a small number. To describe the dynamics before t_m we use a path-integral treatment with the Feynman-Kac formula, denoting the weight of a path in terms of the propagator $\langle x_0|e^{-\hat{H}t_m}|M-\epsilon\rangle$, where $\hat{H} = -\frac{1}{2}\frac{\partial^2}{\partial x^2}$ with $V(x)$ as the potential energy. In the small bubble case the weight of the left path is

$$\begin{aligned} W_L &\propto \exp\left[-\frac{1}{2}\int_0^{t_m} d\tau \left(\frac{dx}{d\tau} + \frac{\tilde{C}_1}{x}\right)^2\right] \\ &= \exp\left[-\tilde{C}_1 \ln\left(\frac{M-\epsilon}{x_0}\right)\right]\langle x_0|e^{-\hat{H}t_m}|M-\epsilon\rangle \\ &= \left(\frac{x_0}{M-\epsilon}\right)^{\tilde{C}_1}\sum_{n=1}^{\infty} e^{-E_p t_m}\psi_n(M-\epsilon)\psi_n(x_0), \end{aligned} \quad (67)$$

where ψ_n and E_n are the eigenfunction and eigenenergies of the Hamiltonian $\hat{H}$ with the eigenvalue equation defined as

$$\left[-\frac{1}{2}\frac{d^2}{dx^2} + \frac{\tilde{C}_1^{\,2}}{2x^2}\right]\psi = E\psi \qquad 0 < x < M. \quad (68)$$

The general solution of the above equation is

$$\psi_n(x) = A\sqrt{x}J_\alpha(\sqrt{2E_n}x) + B\sqrt{x}Y_\alpha(\sqrt{2E_n}x), \quad (69)$$

where $J_\alpha(x)$ and $Y_{-\alpha}(x)$ are the Bessel function of the first and second kind, respectively, of order α and $\alpha = \frac{1}{2}\sqrt{1+4\tilde{C}_1^{\,2}}$, and A and B are arbitrary constants to be determined from the boundary conditions. Utilizing the boundary condition $\psi_n(x=0)=0$, we find that $B=0$. From the second boundary condition $\psi_n(x\to\infty)=0$ we obtain

$$J_\nu(\sqrt{2E_n}M) = 0, \quad (70)$$

which gives us the discrete energy values $\sqrt{2E_n}M = \alpha_{\nu,n}$; $\alpha_{\nu,n}$ are the zeros of the Bessel functions. The particular solutions are therefore given by

$$\psi_n(x) = A\sqrt{x}J_\nu\left(\frac{\alpha_{\nu n}x}{M}\right). \quad (71)$$

Using the normalization condition we can also identify the prefactor, $A = \frac{\sqrt{2}}{MJ_{\nu+1}(\alpha_{\nu,n})}$. Thus, the eigenfunction is given by

$$\psi_n(x) = \frac{\sqrt{2x}}{M|J_{\alpha+1}(u_{\alpha n})|}J_\alpha\left(\frac{u_{\alpha n}x_0}{M}\right). \quad (72)$$

Plugging in the eigenfunctions and eigenenergies in the propagator, the probability W_L in the leading order of ϵ is given by

$$W_L \propto \epsilon\frac{2x_0^{\tilde{C}_1+1/2}}{M^{\tilde{C}_1+5/2}}\sum_{n=1}^{\infty} u_{\alpha n}\frac{e^{-u_{\alpha n}^2 t_m/2M^2}}{J_{\alpha+1}(u_{\alpha n})}J_\alpha\left(\frac{u_{\alpha n}x_0}{M}\right) + O(\epsilon^2). \quad (73)$$

The weight of the complete path in the time domain $[0, t_f]$ with a maximum M at t_m is given by the product of Eqs. (66) and (73),

$$P(M, t_m; \epsilon) = B(\epsilon)W_L W_R, \quad (74)$$

with $B(\epsilon) = \frac{1}{2\epsilon^2}(\frac{x_0}{M})^{C-\tilde{C}_1-1/2}$, where $C = 2\tilde{C}_1 + 1 - \sqrt{1+4\tilde{C}_1^{\,2}}/2$. Finally, the joint probability distribution is given by

$$\begin{aligned} P(M, t_m) &= (2\tilde{C}_1+1)\frac{x_0^C}{M^{C+3}}\sum_{n=1}^{\infty} u_{\alpha n}\frac{e^{-u_{\alpha n}^2 t_m/2M^2}}{J_{\alpha+1}(u_{\alpha n})} \\ &\quad \times J_\alpha\left(\frac{u_{\alpha n}x_0}{M}\right). \end{aligned} \quad (75)$$

It is not possible to calculate the marginal PDF of time at which maximum occurs $P(t_m)$, from Eq. (75). Numerically simulated result of PDF $P(t_m)$ is plotted in Fig. 4(c).

V. CONCLUSIONS

In this work, we analyze several relevant probability distribution functions of various Brownian functionals associated with the stochastic model for the bubble dynamics of DNA, incorporating the effect of an external rapidly oscillating periodic force. Based on the backward Fokker-Planck method discussed in Ref. [36], we derive (i) the first-passage time distribution $P(t_f|x_0)$, providing information about the lifetime of the stochastic process, (ii) the distribution, $P(A|x_0)$, of the area A covered by the random walk until the first passage time, measuring the reactivity of stochastic processes, and (iii) the distribution $P(M)$ of the maximum size M before first passage time, and (iv) the joint probability distribution $P(M; t_m)$ of the maximum size M and the time t_m of its occurrence before the first passage time was also obtained by employing the Feynman-Kac path integral formulation. One can actually advocate for the elegant methods adopted here by stating that the various PDFs for different functionals can be derived by making proper choices of a single term $U(x_0)$ in our parent differential equations (14) and (15) with appropriate boundary conditions. We investigate separately the dynamics of small and large bubbles. Analytical results for the PDFs at each limit nicely match with the Langevin simulations. Our investigation discloses several nontrivial scaling behaviors of $P(t_f|x_0)$, $P(A|x_0)$, $P(M)$, and $P(M, t_m)$, as summarized in Tables I and II below. The scaling

TABLE I. Scaling behavior of the probability distribution function calculated in this work for large and small asymptotes for the case of large bubble dynamics for both periodic driving cases.

Quantities	Large asymptote	Small asymptote
$P(t_f\|x_0) \sim$	$t_f^{-3/2} e^{-C_2 x_0} e^{-C_2^2 t_f/2}$	$\exp[-\frac{(x_0+C_2^2 t_f)^2}{2t_f}]$
$P(A\|x_0) \sim$	$A^{-\frac{3}{4}} e^{-\sqrt{\frac{8AC_2^3}{3}}}$	$A^{-4/3} e^{-2x_0^3/9A}$
$P(M) \sim$	$\sim \frac{1}{\sinh^2(C_2 M)}$	$\frac{1}{(C_2 M)^2}$
$P(t_m) \sim$	$t_m^{-\frac{5}{6}} \exp(-\frac{C_2^2 t_m}{2} - \frac{3}{2}[C_2\pi]^{2/3} t_m^{1/3})$	$t_m^{-1/2}$

TABLE II. Scaling behavior of the probability distribution function calculated in this work for large and small asymptotes for the case of small bubble dynamics for periodic driving $F(x,t) = f_0 \cos(\omega t)$ (case I). The numerically fitted result in the large asymptote for the periodic driving $F(x,t) = f_0 x \cos(\omega t)$ is the same as that of case I.

Quantities	Large asymptote	Small asymptote
$P(t_f\|x_0) \sim$	$t_f^{-\tilde{C}_1 - 3/2}$	$e^{-x_0^2/2t_f}$
$P(A\|x_0) \sim$	$A^{-\frac{2}{3}(\tilde{C}_1+2)}$	$e^{-2x_0^3/9A}$
$P(M) \sim$	$M^{-2\tilde{C}_1 - 2}$	$M^{-2\tilde{C}_1 - 2}$
$P(t_m) \sim$	$t_m^{-\tilde{C}_1 - 3/2}$	Not known

exponents are specified either by the entropic parameter $C_1 = c/2$ or by the base-pair dissociation parameter $C_2 = \gamma(T - T_m)/(2k_b T T_m)$ and rapidly oscillating force modified entropic parameter $\tilde{C}_1 = C_1(1 + \frac{f_0^2}{2\omega^2})$. Thus, all these PDFs can be measured experimentally by using fluorescence correlation spectroscopy [24], e.g., the maximum size distribution $P(M)$ for small and large bubbles separately. We expect our results to be useful in quantifying chemical processes within DNA, for example, protein binding to single-stranded DNA, and for developing a deeper understanding of polymer dynamics. It is of interest to extend our study and consider loop-loop interactions [53] and the effects of disorder and heterogeneity in predicting the kinetics of specific processes within DNA bubbles.

Finally, our present work, is the extension of the previous work on Brownian functionals [63] on DNA bubble dynamics by incorporating the effect of two different types of external rapidly oscillating forces. Our main observation from this study is that the DNA bubble dynamics for the large bubble size is unaffected by a rapidly oscillating time periodic force in timescales larger than $\tilde{T} = \frac{2\pi}{\omega}$. On the other hand, the small bubble dynamics is significantly affected by the external periodic force (see the scaling behavior in table).

[1] D. Marks, J. Kimball, D. Tingey, and T. Link, Hydrol. Process. **12**, 1569 (1998).

[2] A. Hamlet and D. Lettenmaier, J. Am. Water Resour. Assoc. **35**, 1597 (1999).

[3] M. Pascual, M. Bouma, and A. Dobson, Microbes Infect. **4**, 237 (2002).

[4] J. Patz, D. Campbell-Lendrum, T. Holloway, and J. Foley, Nature (London) **438**, 310 (2005).

[5] C. Barranguet, J. Kromkamp, and J. Peene, Mar. Ecol.: Prog. Ser. **173**, 117 (1998).

[6] M. Bertness and G. Leonard, Ecology **78**, 1976 (1997).

[7] H. Charles and J. S. Dukes, Ecol. Appl. **19**, 1758 (2009).

[8] A. R. Bulsara, S. B. Lowen, and C. D. Rees, Phys. Rev. E **49**, 4989 (1994).

[9] A. R. Bulsara, T. C. Elston, C. R. Doering, S. B. Lowen, and K. Lindenberg, Phys. Rev. E **53**, 3958 (1996).

[10] H. E. Plesser and S. Tanaka, Phys. Lett. A **225**, 228 (1997); J. R. R. Duarte, M. V. D. Vermelho, and M. L. Lyra, Physica A (Amsterdam) **387**, 1446 (2008).

[11] R. J. Williams, *Introduction to the Mathematics of Finance* (American Mathematical Society, Providence, RI, 2006).

[12] M. Yor, *Exponential Functionals of Brownian Motion and Related Topics* (Springer, Berlin, 2000).

[13] E. Urdapilleta, Phys. Rev. E **83**, 021102 (2011).

[14] J. Benda, L. Maler, and A. Longtin, J. Neurophysiol. **104**, 2806 (2010); B. Lindner and A. Longtin, J. Theor. Biol. **232**, 505 (2005).

[15] S. Kumar and G. Mishra, Phys. Rev. Lett. **110**, 258102 (2013); S. Kumar, R. Kumar, and W. Janke, Phys. Rev. E **93**, 010402(R) (2016).

[16] B. S. Alexandrov, V. Gelev, A. R. Bishop, A. Usheva, and K. Ø. Rasmussen, Phys. Lett. A **374**, 1214 (2010).

[17] E. S. Swanson, Phys. Rev. E **83**, 040901(R) (2011).

[18] A. Molini, P. Talkner, G. G. Katul, and A. Porporatoa, Physica A (Amsterdam) **390**, 1841 (2011).

[19] R. M. Wartell and A. S. Benight, Phys. Rep. **126**, 67 (1985).

[20] D. Poland and H. A. Scheraga, *Theory of the Helix-Coil Transition in Bio- Polymers* (Academic, New York, 1970).

[21] C. Danilowicz, Y. Kafri, R. S. Conroy, V. W. Coljee, J. Weeks, and M. Prentiss, Phys. Rev. Lett. **93**, 078101 (2004).

[22] N. K. Voulgarakis, A. Redondo, A. R. Bishop, and K. Ø. Rasmussen, Phys. Rev. Lett. **96**, 248101 (2006).

[23] R. Metzler, T. Ambjörnsson, A. Hanke, and H. C. Fogedby, J. Phys.: Condens. Matter **21**, 034111 (2009), and references therein.

[24] O. Krichevsky and G. Bonnet, Rep. Prog. Phys. **65**, 251 (2002).

[25] G. Altan-Bonnet, A. Libchaber, and O. Krichevsky, Phys. Rev. Lett. **90**, 138101 (2003).

[26] T. Ambjörnsson and R. Metzler, Phys. Rev. E **72**, 030901(R) (2005).

[27] H. Kunz, R. Livi, and A. Süto, J. Stat. Mech.: Theory Exp. (2007) P06004.

[28] T. Ambjörnsson, S. K. Banik, M. A. Lomholt, and R. Metzler, Phys. Rev. E **75**, 021908 (2007).

[29] S. K. Banik, T. Ambjörnsson, and R. Metzler, Europhys. Lett. **71**, 852 (2005).

[30] A. Hanke and R. Metzler, J. Phys. A **36**, L473 (2003).

[31] A. Bar, Y. Kafri, and D. Mukamel, Phys. Rev. Lett. **98**, 038103 (2007).

[32] T. Dauxois, M. Peyrard, and A. R. Bishop, Phys. Rev. E **47**, 684 (1993).

[33] S. Srivastava and Y. Singh, Europhys. Lett. **85**, 38001 (2009).

[34] H. C. Fogedby and R. Metzler, Phys. Rev. Lett. **98**, 070601 (2007); Phys. Rev. E **76**, 061915 (2007).
[35] L.-A. Wu, S. S. Wu, and D. Segal, Phys. Rev. E **79**, 061901 (2009).
[36] S. N. Majumdar, Curr. Sci. **89**, 2076 (2005).
[37] A. Comtet, C. Monthus, and M. Yor, J. Appl. Probab. **35**, 255 (1998).
[38] M. J. Kearney, J. Phys. A **37**, 8421 (2004).
[39] J. Randon-Furling and S. N. Majumdar, J. Stat. Mech.: Theory Exp. (2007) P10008.
[40] M. Kac, Trans. Am. Math. Soc. **65**, 1 (1949).
[41] S. N. Majumdar and M. J. Kearney, Phys. Rev. E **76**, 031130 (2007).
[42] P. L. Krapivsky, S. N. Majumdar, and A. Rosso, J. Phys. A **43**, 315001 (2010).
[43] S. Chandrasekhar, Rev. Mod. Phys. **15**, 1 (1943).
[44] H. Risken, *The Fokker-Planck Equation: Methods of Solutions and Applications*, 2nd ed. (Springer-Verlag, Berlin, 1989).
[45] C. W. Gardiner, *Handbook of Stochastic Methods: For Physics, Chemistry and the Natural Sciences*, 2nd ed. (Springer-Verlag, Berlin, 1985).
[46] A. Bar, Y. Kafri, and D. Mukamel, J. Phys.: Condens. Matter **21**, 034110 (2009).
[47] S. K. Sarkar and S. Dattagupta, Int. J. Mod. Phys. B **16**, 1247 (2002).
[48] *Collected Papers of P. L. Kapitza*, edited by D. ter Haar (Pergamon, Oxford, 1964); P. L. Kapitza, Zh. Eksp. Teor. Fiz. **21**, 588 (1951).
[49] L. D. Landau and E. M. Lifshitz, *Mechanics* (Pergamon, Oxford, 1976).
[50] S. Rahav, E. Geva, and S. Fishman, Phys. Rev. E **71**, 036210 (2005).
[51] S. Rahav, I. Gilary, and S. Fishman, Phys. Rev. Lett. **91**, 110404 (2003).
[52] P. Jung, Z. Phys. B **76**, 521535 (1989).
[53] Y. Kafri, D. Mukamel, and L. Peliti, Physica A (Amsterdam) **306**, 39 (2002).
[54] A. Ridinger and C. Weiss, Phys. Rev. A **79**, 013414 (2009).
[55] T. Junglen, T. Rieger, S. A. Rangwala, P. W. H. Pinkse, and G. Rempe, Phys. Rev. Lett. **92**, 223001 (2004).
[56] J. van Veldhoven, H. L. Bethlem, and G. Meijer, Phys. Rev. Lett. **94**, 083001 (2005).
[57] N. G. van Kampen, *Stochastic Processes in Physics and Chemistry* (North-Holland, Amsterdam, 2007).
[58] A. C. Branka and D. M. Heyes, Phys. Rev. E **58**, 2611 (1998).
[59] *Tables of Integral Transforms*, Based, in part, on notes left by Harry Bateman and compiled by the staff of the Bateman Manuscript Project, edited by A. Erdelyi, M. F. Oberhettinger, and F. G. Tricomi (McGraw-Hill, New York, 1954), Vol. I.
[60] G. B. Arfken and H. J. Weber, *Mathematical Methods for Physicists*, 4th ed. (Academic Press, London, 1995).
[61] M. Abramowitz and I. A. Stegun, *Handbook of Mathematical Functions* (Dover, New York, 1973).
[62] I. S. Gradshteyn and I. M. Ryzhik, *Tables of Integrals, Series, and Products* (Academic Press, New York, 1965).
[63] M. Bandyopadhyay, S. Gupta, and D. Segal, Phys. Rev. E **83**, 031905 (2011).